

## Photoionization branching ratios of spin-orbit doublets far above thresholds: Interchannel and relativistic effects in the noble gases

C. Rasadi Munasinghe<sup>1</sup>, Pranawa C. Deshmukh<sup>2,3</sup> and Steven T. Manson<sup>1</sup>

<sup>1</sup>*Department of Physics and Astronomy, Georgia State University, Atlanta, Georgia 30030, USA*

<sup>2</sup>*Department of Physics and CAMOST, Indian Institute of Technology Tirupati, Tirupati 517506, India*

<sup>3</sup>*Department of Physics, Dayananda Sagar University, Bangalore 560114, India*



(Received 23 February 2022; accepted 16 June 2022; published 5 July 2022)

Photoionization branching ratios of all of the spin-orbit doublets in the noble gas atoms Ne, Ar, Kr, and Xe have been investigated theoretically at energies well above the thresholds. The results confirm in all cases that the general behavior of the branching ratios is to decrease monotonically below their statistical value with increasing photon energy. This effect gets more pronounced with increasing  $Z$ . In addition, the branching ratios can be strongly affected by interchannel coupling with inner shell photoionization channels. Although these effects are strongest in the neighborhood of the inner shell thresholds, they can persist over a broad range of energies,

DOI: [10.1103/PhysRevA.106.013102](https://doi.org/10.1103/PhysRevA.106.013102)

### I. INTRODUCTION

The photoionization process is an excellent tool for the study of atomic dynamics owing to the weakness of the photon-electron interaction along with the fact that the photon disappears after the interaction [1]. Over the years, the study of relativistic interactions in many aspects of the photoionization of atoms has received significant scrutiny [2–14]. A particularly interesting case is the branching ratios (BRs) of the cross sections of spin-orbit doublets. From a nonrelativistic point of view, the photoionization branching ratio of a  $nl$  doublet,  $(j = l + 1)/(j = l - 1)$  approaches  $(l + 1)/l$ , known as the statistical ratio, that simply reflects the occupancy to the two  $j$  states [15]. At low energies, near the thresholds, the branching ratios can vary owing to the fact that the photoelectrons from each member of a doublet have different energies; this is known as the kinetic energy effect [16–19]. At energies far above the thresholds, where the photoelectron energies are quite large, the kinetic energy difference becomes unimportant since the spin-orbit splitting is very small compared to the photoelectron energies, and the only possibility for deviation from the statistical ratio is the effect(s) of relativistic interactions.

Some time ago, it was predicted theoretically that the relativistic effects on the wave functions would cause the branching ratios to deviate from the statistical ratios. Specifically, it was shown that the branching ratio would not go to a limit at all but would continually decrease with energy as a result of the relativistic alteration of the initial-state wave functions [20,21], but this prediction could not be verified at the time with the then extant level of experimental capability. However, with recent advances in experimental technology, the prediction has recently been verified in the laboratory [22]. In addition, it has been found that, in the neighborhood of inner-shell thresholds, relativistic effects on the interchannel

coupling cause significant alterations in the branching ratio [22,23], i.e., the interchannel interactions can be very different for the two members of a spin-orbit doublet owing to relativistic effects.

In order to understand how these various effects behave as functions of energy, subshell, and  $Z$ , and where the various physical interactions are important, we have embarked upon a computational study of the noble gases, Ne, Ar, Kr, and Xe including all subshells and over a broad range of photon energy. A further motivation for this work is to provide a road map for experiment which is currently possible. The relativistic-random-phase approximation (RRPA), which is based on the Dirac equation so that relativistic interactions are included on an *ab initio* basis, is employed in the calculation [24,25]. RRPA also includes significant initial discrete and final continuum state correlations. In particular RRPA contains the interchannel coupling among the final-state channels which essentially amounts to configuration interaction in the continuum [24,25]. At the low energies, it has been shown that the RRPA does an excellent job of reproducing the experimental branching ratios [4]; it is, therefore, reasonable to assume that the RRPA predictions at high energies are also accurate. This has been already tested in several cases [22].

Section II presents a brief discussion of the RRPA along with the details of the present calculations. Section III presents and discusses the branching ratio results on Ne, Ar, Kr, and Xe, and the final section gives a summary and conclusions.

### II. THEORY AND DETAILS OF THE CALCULATION

The relativistic-random-phase approximation (RRPA) [24,25] has been used to perform the calculations. The RRPA methodology is well known so it will not be repeated in detail here. It is based on the Dirac equation so that relativistic

tic effects, including the spin-orbit interaction, are included on an *ab initio* basis. In addition, initial-state two-particle two-hole correlations are included in the RRPA, as well as final-state correlations in the form of interchannel coupling (configuration interaction in the continuum). The importance of interchannel coupling rests on the idea that photoionizing transitions (channels) with a small cross section that are degenerate with channels having a large cross section can be strongly affected by the mixing of the final-state continuum wave functions induced by the coupling. Furthermore, interchannel coupling can even dominate the cross section of the weak channel. Numerous situations exist in which this has been documented in both theoretical and experimental studies, e.g., [22,26,27].

The RRPA has, of course, certain limitations. Some types of multiple excitations from the initial state, e.g., ionization plus excitation channels, are not included. However, since these multiple excitation or ionization cross sections are small compared to the cross sections of single-ionization channels, a perturbation theory argument [26,27] indicates that they do not play a strong role in the interchannel coupling of the cross sections of interest and thus on the branching ratios. Furthermore, resonance regions are not done well owing to the absence of spectator Auger channels. These channels come into play when an inner-shell electron is excited by the incident photon and the subsequent Auger decay does not involve that same excited electron, leaving the residual ion in an excited state [28]. In addition, Dirac-Fock energies are used which can be a bit off particularly for inner shells. But this leads only to small energy level shifts and will result in no significant dynamical effects in the cross sections and branching ratios. Similarly, the omission of the Breit interaction and QED lead to only very small energy shifts and essentially no dynamical effects. As far as we are aware there has been no published work that has considered the effects of these small interactions on dipole photoionization transition matrix elements, thereby suggesting that the effects are negligible. The RRPA method has an important property: the matrix elements and cross sections are gauge-independent, i.e., length and velocity photoionization matrix elements are equal [25]. Technically, however, this only applies when all dipole allowed single-excitation channels are included. By truncating the RRPA calculation, coupling only some of the channels, it is possible to pinpoint the specific channels responsible for the interchannel coupling, in any given case.

Calculations were performed including all single-excitation relativistic dipole photoionization channels for Ne, Ar, Kr, and Xe, except that for Xe the  $1s$  photoionization channels were omitted, since the  $1s$  ionization threshold is so high in energy. A simple perturbation theory argument demonstrates that the omission will have negligible impact on the results at the energies considered. The fully coupled calculations included

Ne:  $2p_{3/2} \rightarrow s_{1/2}, d_{3/2}, d_{5/2}$ ;  $2p_{1/2} \rightarrow s_{1/2}, d_{3/2}$ ;  $2s \rightarrow p_{1/2}, p_{3/2}$ ;  $1s \rightarrow p_{1/2}, p_{3/2}$  (nine channels).

Ar:  $3p_{3/2} \rightarrow s_{1/2}, d_{3/2}, d_{5/2}$ ;  $3p_{1/2} \rightarrow s_{1/2}, d_{3/2}$ ;  $3s \rightarrow p_{1/2}, p_{3/2}$ ;  $2p_{3/2} \rightarrow s_{1/2}, d_{3/2}, d_{5/2}$ ;  $2p_{1/2} \rightarrow s_{1/2}, d_{3/2}$ ;  $2s \rightarrow p_{1/2}, p_{3/2}$ ;  $1s \rightarrow p_{1/2}, p_{3/2}$  (16 channels).

Kr:  $4p_{3/2} \rightarrow s_{1/2}, d_{3/2}, d_{5/2}$ ;  $4p_{1/2} \rightarrow s_{1/2}, d_{3/2}$ ;  $4s \rightarrow p_{1/2}, p_{3/2}$ ;  $3d_{5/2} \rightarrow p_{3/2}, f_{5/2}, f_{7/2}$ ;  $3d_{3/2} \rightarrow p_{1/2}, p_{3/2}, f_{5/2}$ ;

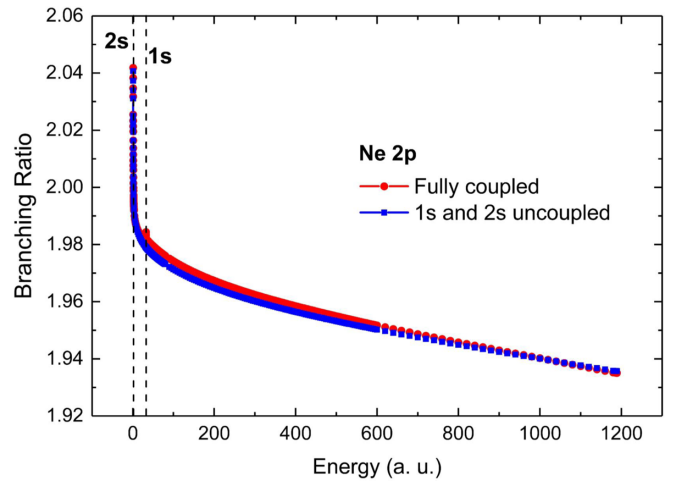


FIG. 1. Photoionization cross section branching ratio for Ne  $2p_{3/2}/2p_{1/2}$  calculated using RRPA with full coupling (red dots) and without coupling to  $1s$  and  $2s$  channels (blue squares). The vertical dashed lines indicate the thresholds.

$3p_{3/2} \rightarrow s_{1/2}, d_{3/2}, d_{5/2}$ ;  $3p_{1/2} \rightarrow s_{1/2}, d_{3/2}$ ;  $3s \rightarrow p_{1/2}, p_{3/2}$ ;  
 $2p_{3/2} \rightarrow s_{1/2}, d_{3/2}, d_{5/2}$ ;  $2p_{1/2} \rightarrow s_{1/2}, d_{3/2}$ ;  $2s \rightarrow p_{1/2}, p_{3/2}$ ;  
 $1s \rightarrow p_{1/2}, p_{3/2}$  (29 channels).

Xe:  $5p_{3/2} \rightarrow s_{1/2}, d_{3/2}, d_{5/2}$ ;  $5p_{1/2} \rightarrow s_{1/2}, d_{3/2}$ ;  $5s \rightarrow p_{1/2}, p_{3/2}$ ;  
 $4d_{5/2} \rightarrow p_{3/2}, f_{5/2}, f_{7/2}$ ;  $4d_{3/2} \rightarrow p_{1/2}, p_{3/2}, f_{5/2}$ ;  
 $4p_{3/2} \rightarrow s_{1/2}, d_{3/2}, d_{5/2}$ ;  $4p_{1/2} \rightarrow s_{1/2}, d_{3/2}$ ;  $4s \rightarrow p_{1/2}, p_{3/2}$ ;  
 $3d_{5/2} \rightarrow p_{3/2}, f_{5/2}, f_{7/2}$ ;  $3d_{3/2} \rightarrow p_{1/2}, p_{3/2}, f_{5/2}$ ;  $3p_{3/2} \rightarrow s_{1/2}, d_{3/2}, d_{5/2}$ ;  
 $3p_{1/2} \rightarrow s_{1/2}, d_{3/2}$ ;  $3s \rightarrow p_{1/2}, p_{3/2}$ ;  $2p_{3/2} \rightarrow s_{1/2}, d_{3/2}, d_{5/2}$ ;  
 $2p_{1/2} \rightarrow s_{1/2}, d_{3/2}$ ;  $2s \rightarrow p_{1/2}, p_{3/2}$  (40 channels).

In addition, in most cases, truncated RRPA calculations were performed with only specific interchannel couplings included to understand how important the interchannel coupling is, and the coupling between which specific channels is the crucial one (or ones) in particular situations.

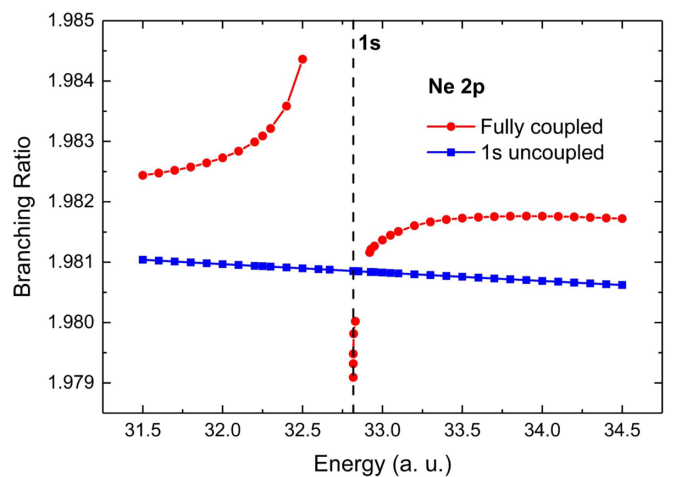


FIG. 2. Photoionization cross section branching ratio for Ne  $2p_{3/2}/2p_{1/2}$  calculated using RRPA with full coupling (red dots) and without coupling to  $1s$  channels (blue squares). The vertical dashed line indicates the  $1s$  threshold.

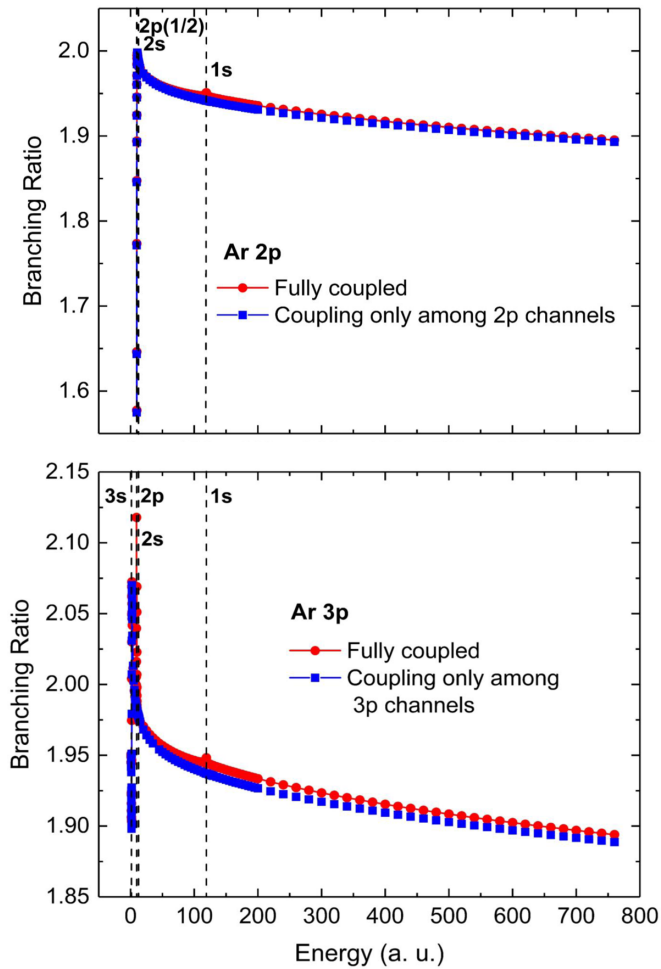


FIG. 3. Photoionization cross section branching ratios for Ar  $2p_{3/2}/2p_{1/2}$  (upper panel) and  $3p_{3/2}/3p_{1/2}$  (lower panel) calculated using RRPA with full coupling (red dots) and with coupling only among  $2p$  and  $3p$  channels, respectively (blue squares). The vertical dashed lines indicate the thresholds.

### III. RESULTS AND DISCUSSION

#### A. Ne

Looking first at Ne, the lowest- $Z$  element studied with all relativistic photoionization channels from the  $1s$ ,  $2s$ , and  $2p$  subshells coupled in the calculation, Fig. 1 depicts the broad behavior of the  $2p_{3/2}/2p_{1/2}$  photoionization branching ratio. As a result of the equality of length and velocity gauges in the RRPA, only a single curve (the velocity form) is shown for each case for Ne and for all subsequent calculations. In any case, Fig. 1 shows that the branching ratio clearly does not go to a statistical ratio of 2 with increasing photon energy; the effects of the relativistic modification of the  $2p$  wave functions on the branching ratio are evident in that the branching ratio moves below 2 and continues decreasing with increasing photon energy. The origin of this general phenomenology was predicted earlier [20,21]; it is useful to understand in detail the underlying cause. To begin with, as the energy of a photoionizing transition increases, the dipole matrix is generated closer and closer to the nucleus, and this can be understood both mathematically and physically. From a mathematical standpoint, with increasing photoelectron energy the continuum wave function (the final state of the photoelectron after photoabsorption) becomes increasingly oscillatory, resulting in a net cancellation of the matrix element beyond the first node of the continuum wave function. This node moves towards the nucleus with increasing energy, thereby causing the matrix element to be generated in a region increasingly close to the nucleus as the energy increases. From a physical point of view, both energy and linear momentum must be conserved in the photoionization process. High-energy photoabsorption entails a lot of linear momentum which must be transferred to the residual atom, where most of the mass is at the nucleus. Thus, to take up this momentum, the absorption is most likely to take place near the nucleus, i.e., at small  $r$ .

In any case, at large distances from the nucleus (large  $r$ ) the  $2p_{3/2}$  and  $2p_{1/2}$  wave functions are virtually identical, but this

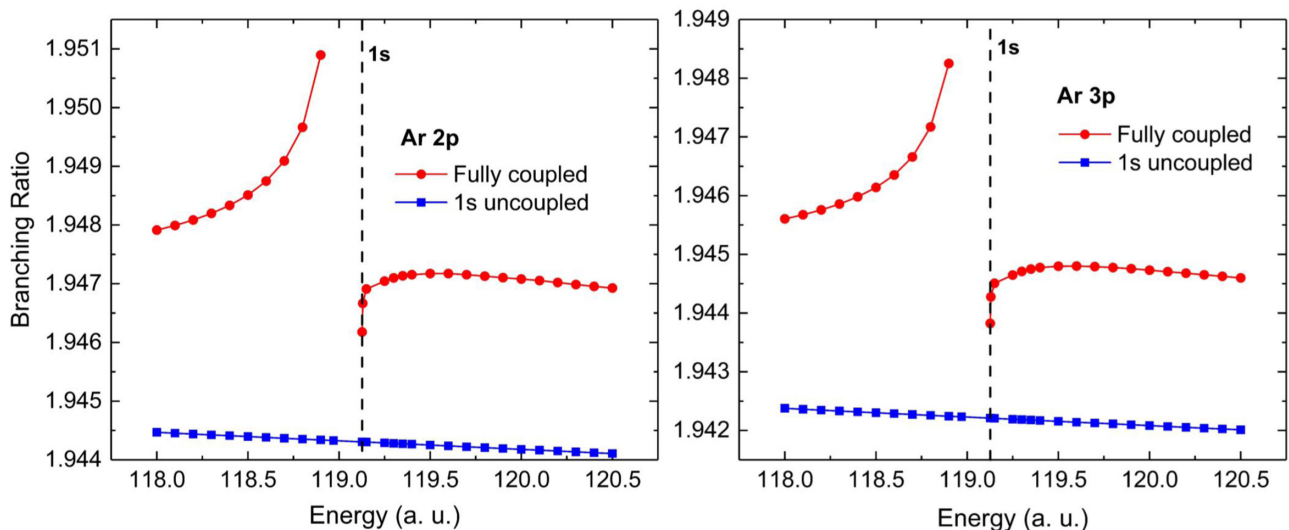


FIG. 4. Photoionization cross section branching ratios for Ar  $2p_{3/2}/2p_{1/2}$  (left panel) and  $3p_{3/2}/3p_{1/2}$  (right panel) in the vicinity of the Ar  $1s$  threshold calculated using RRPA with full coupling (red dots) and with coupling only among  $2p$  and  $3p$  channels (blue squares), respectively. The vertical dashed lines indicate the  $1s$  threshold.

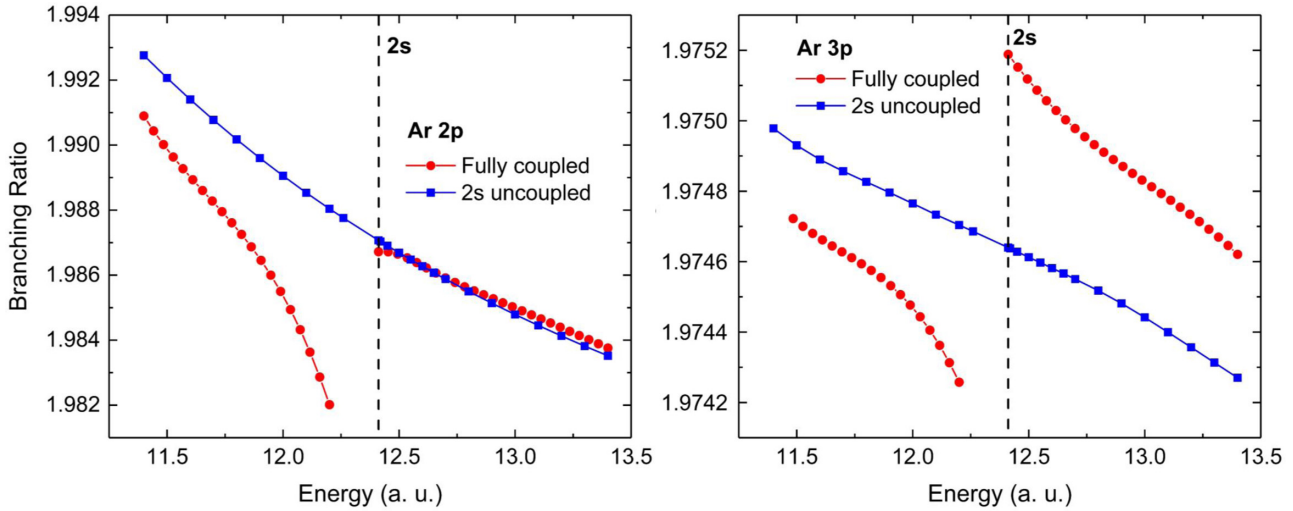


FIG. 5. Photoionization cross section branching ratios for Ar  $2p_{3/2}/2p_{1/2}$  (left panel) and  $3p_{3/2}/3p_{1/2}$  (right panel) in the vicinity of the Ar  $2s$  threshold calculated using RRPAs with full coupling (red dots) and with coupling only among  $2p$  and  $3p$  channels (blue squares), respectively. The vertical dashed lines indicate the  $1s$  threshold.

is not the case for small  $r$  since the behavior of wave functions near the nucleus is determined by  $j$ , not  $l$ , as shown by the Dirac equation [29]. Specifically, the Dirac equation demonstrates that the ratio of probability densities of any spin-orbit doublet  $nl_{l-1/2} : nl_{l+1/2}$  diverges as  $Z^2/r^2$  as  $r \rightarrow 0$ . Thus, the increase of the radial  $j = l - 1/2$  wave function relative to the  $j = l + 1/2$  near the nucleus accounts for the deviation of the branching ratio from the statistical value. As discussed above, since the dipole matrix element is generated at small and smaller  $r$ , with increasing energy, this effect will increase with energy, just as seen for the Ne  $2p_{3/2}/2p_{1/2}$  photoionization branching ratio in Fig. 1. In addition, this suggests that the effects should increase with increasing nuclear charge  $Z$ .

Also shown in Fig. 1 is the  $2p$  branching ratio calculated with no interchannel coupling from  $1s$  and  $2s$  channels, a truncated RRPAs calculation, which shows that interchannel coupling has a small effect over a very large energy range. This reinforces an earlier conclusion that interchannel coupling affects most subshells of most atoms over a range of energies [26,27] with the added dimension that the interchannel coupling is affected by relativistic interactions as well.

A small kink is seen in Fig. 1 around the  $1s$  threshold, shown in greater detail in Fig. 2. From this figure, interchannel coupling is seen to have a small effect in the vicinity of the  $1s$  threshold. Below the threshold the rise in the branching ratio is due to the beginning of the autoionizing resonance region of  $2p \rightarrow ns$  and  $nd$  resonances; the region left blank is fraught with resonances and are not included in this study. Above the  $1s$  threshold, there is a small rise in the branching ratio, thereby indicating that the interchannel coupling affects the  $2p_{3/2}$  and the  $2p_{1/2}$  cross sections differently, i.e., the interchannel coupling is affected by relativistic interactions. Also shown in Fig. 2 is the truncated calculation omitting the coupling with the  $1s$  channels which is quite smooth through this region. This clearly demonstrates that the structure is due to interchannel coupling. Even though the  $1s$  cross section is

much larger than the  $2p$  cross section in this energy region, the effect of the interchannel coupling is quite small. This is because the radial overlap between the  $2p$  and  $1s$  wave functions is small. Still, it is interesting to note that even for low nuclear charges, relativistic effects are evident. This is in line with earlier studies that have demonstrated relativistic effects for even lighter elements [30–32].

### B. Argon

Going up in  $Z$  to argon,  $Z = 18$ , Fig. 3 shows the broad behavior of the Ar  $2p$  and  $3p$  branching ratios in which all relativistic photoionization channels from  $1s$ ,  $2s$ ,  $2p$ ,  $3s$ , and  $3p$  are coupled in the calculation. A small portion of the Ar  $2p$

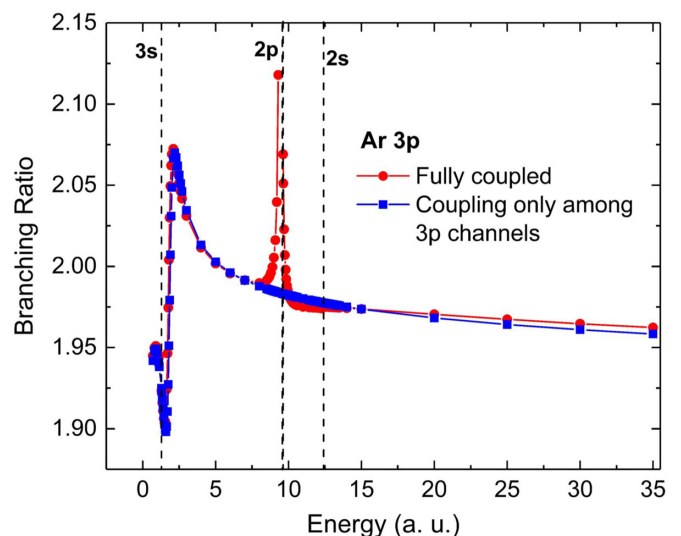


FIG. 6. Photoionization cross section branching ratio for Ar  $3p_{3/2}/3p_{1/2}$  calculated using RRPAs with full coupling (red dots) and with coupling only among  $3p$  channels (blue squares). The vertical dashed lines indicate the thresholds.

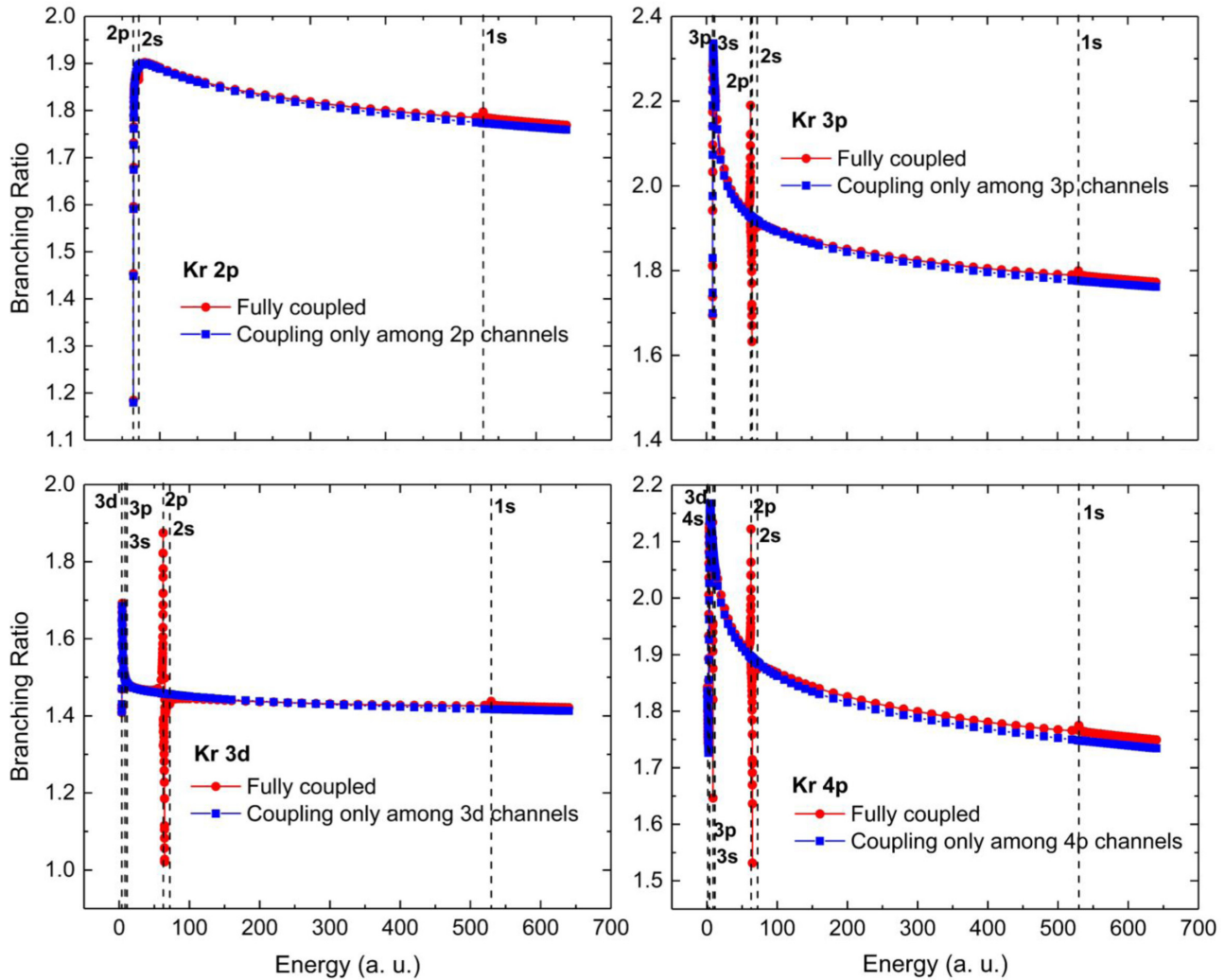


FIG. 7. Photoionization cross section branching ratios for Kr  $np_{3/2}/np_{1/2}$  and  $3d_{5/2}/3d_{3/2}$  calculated using RRPA with full coupling (red dots) and with only intrashell coupling (blue squares). The vertical dashed lines indicate the thresholds.

results were presented earlier [22], but they are also included here for completeness. In any case, while the branching ratios differ in the two cases at low energies, at the higher energies they are remarkably similar, indicating that the principal quantum number of the initial state is not important for the high-energy behavior of the branching ratio. This is because the high-energy dipole matrix elements are generated close to the nucleus, i.e., at small  $r$ . In this region, the nuclear potential is quite large so that the binding energies are essentially irrelevant. In such a region of space the wave functions of the different initial states of the same  $l$  are the same, except for an overall normalization factor [2,33,34], and this normalization factor drops out in the ratio, thus causing the high-energy branching ratios for spin-orbit doublets of the same  $l$  to be essentially the same, exactly as our results indicate. The Ar  $2p$  and  $3p$  branching ratios are also seen to fall off with increasing energy as did the Ne  $2p$ , however they fall off much faster. For example, at a photon energy of 800 a.u., the Ne ratio was about 1.95, while the Ar ratios are about 1.90, thereby indicating that this relativistic effect grows with nuclear charge. This is expected since, as mentioned, the high-energy dipole matrix element is generated quite close to the nucleus. The difference

between the fully coupled branching ratios and the ones with only coupling with the channels from the particular subshell (intrashell coupling), also shown in Fig. 3, is much larger in Ar. This difference is pervasive over a much larger energy range than in Ne, thereby indicating that interchannel coupling is more important in Ar than in Ne. It is noteworthy that experimental results (not shown) for the  $2p$  branching ratio over the photon energy region from about 100 to 150 a.u. have exhibited good agreement with the RRPA results, both in absolute values and the decrease of the ratio with energy [22]. This indicates the overall accuracy of the present results.

Figure 4 shows the Ar  $2p$  and  $3p$  branching ratios in the vicinity of the  $1s$  threshold, along with the results including only intrashell coupling, and, similar to the Ne  $2p$  case, effects of interchannel coupling are exhibited, but are about a factor of 2 smaller than in Ne. This occurs because the  $1s$  orbital in Ar is so compact that there is almost no overlap with the higher orbital, thus making the interchannel coupling matrix element quite small. In the vicinity of the Ar  $2s$  threshold, Fig. 5, there is only a small interchannel coupling effect on the  $2p$  branching ratio because here the  $2s$  cross section is smaller than the  $2p$  cross sections and the  $2s$  threshold is really in the

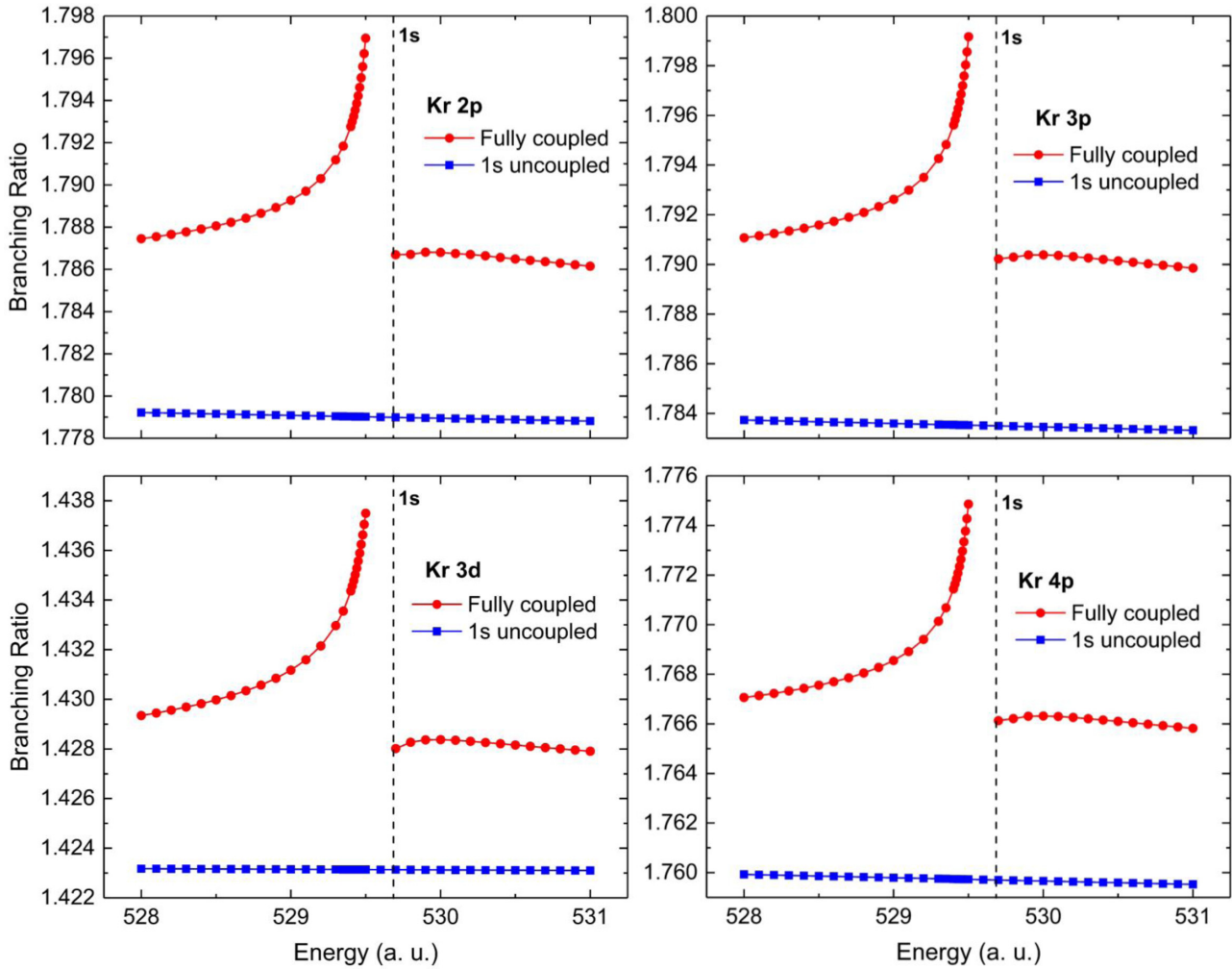


FIG. 8. Photoionization cross section branching ratios for Kr  $np_{3/2}/np_{1/2}$  and  $3d_{5/2}/3d_{3/2}$  in the vicinity of the Kr  $1s$  threshold calculated using RRPA with full coupling (red dots) and truncated RRPA omitting the coupling with the  $1s$  photoionization channels (blue squares). The vertical dashed lines indicate the  $1s$  threshold.

$2p$  threshold region. The results are rather different for the  $3p$  branching ratio for which the  $2s$  threshold region is well above the  $3p$  thresholds. Thus, while the  $2p$  and  $3p$  branching ratios are essentially the same at high energy, they are not so near the  $2s$  threshold owing to the  $2s$  threshold being so close to the  $2p$  thresholds. It is also evident that the deviation of the fully coupled ratios from the truncated intrashell results differ qualitatively for this same reason.

Figure 6 depicts a closeup of the Ar  $3p$  branching ratio at the lower energies where the strong effects of the coupling with the  $2p$  photoionization channels in the vicinity of the  $2p$  thresholds is seen. Near threshold, the situation has been discussed earlier and good agreement with earlier calculations is found (not shown) [4,35]; there does not appear to be significant experimental data for the Ar  $3p$  branching ratio, probably due to the small splitting of about 0.177 eV between  $3p_{3/2}$  and  $3p_{1/2}$  [36]. There is a very significant variation in the  $3p$  branching ratio in the vicinity of the  $2p$  thresholds, as is clearly demonstrated by the qualitative differences in the fully coupled and the truncated intrashell branching ratios in this region. This suggests that there is significant interchannel coupling among  $np$  channels, and that this interchannel cou-

pling is strongly affected by relativistic interactions, i.e., the coupling is strongly  $j$  dependent.

### C. Krypton

The Kr calculations include all of the photoionization channels from  $1s$ ,  $2s$ ,  $2p$ ,  $3s$ ,  $3p$ ,  $3d$ ,  $4s$ , and  $4p$  subshells, a total of 29 coupled relativistic channels. An overall view of the  $2p$ ,  $3p$ ,  $4p$ , and  $3d$  branching ratios is shown in Fig. 7. For the  $np$  states, at the highest energies of 650 a.u., the branching ratios are about 1.8, continuing the trend seen for Ne and Ar that the asymptotic branching ratios decrease with nuclear charge owing to the increased relativistic effects associated with higher  $Z$ . Also, as seen and explained in the Ar case, the high-energy branching ratios are largely independent of the principal quantum number  $n$  of the initial  $np$  state (note the differing vertical scales on the various plots). Furthermore, continuing the trend seen for Ne and Ar, the difference between the fully coupled branching ratios and the truncated ones with only coupling with the channels from the particular subshell (intrashell coupling) is much larger in Kr. This

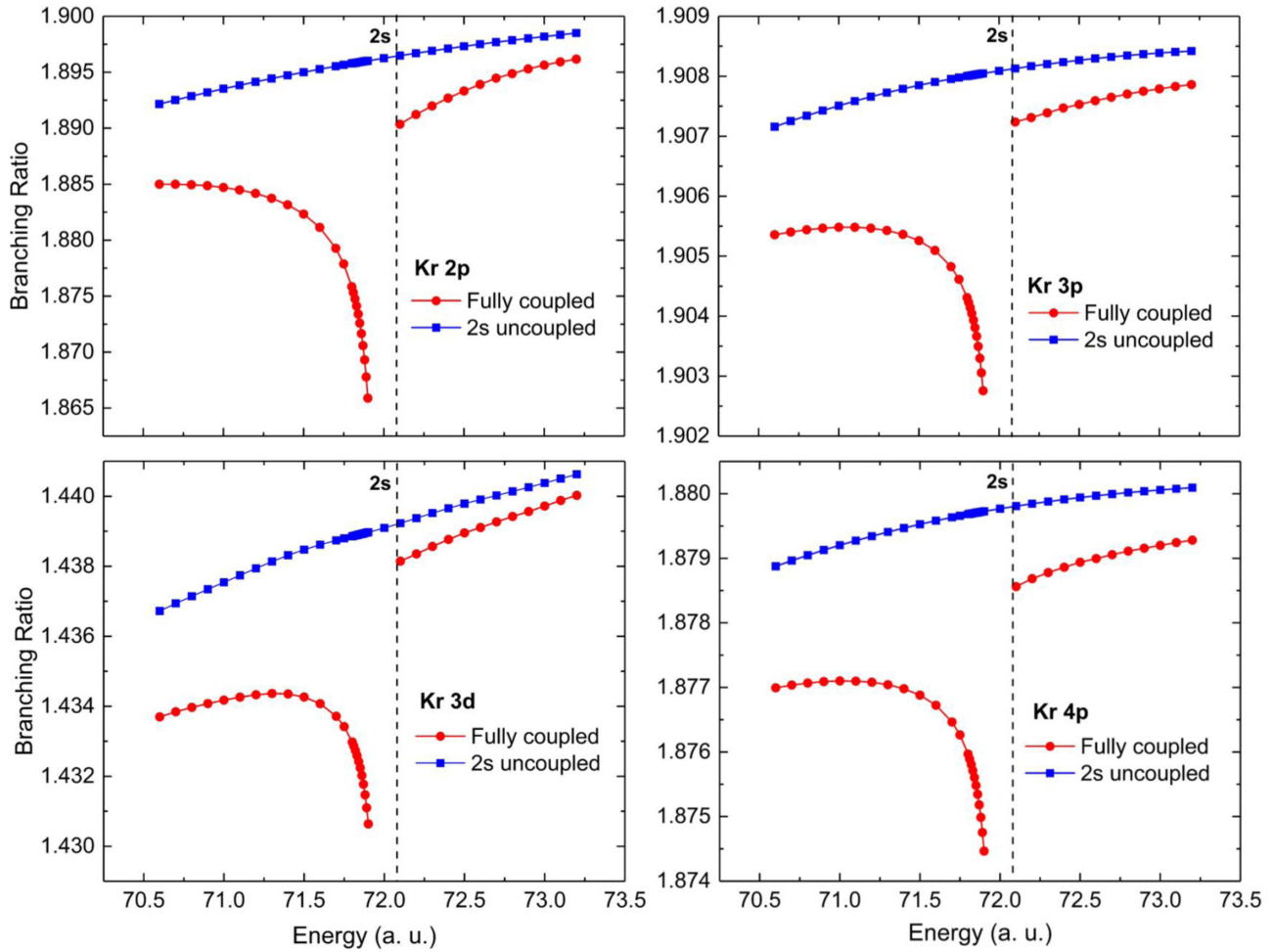


FIG. 9. Photoionization cross section branching ratios for Kr  $np_{3/2}/np_{1/2}$  and  $3d_{5/2}/3d_{3/2}$  in the vicinity of the Kr  $2s$  threshold calculated using RRPA with full coupling (red dots) and truncated RRPA omitting the coupling with the  $2s$  photoionization channels (blue squares). The vertical dashed lines indicate the  $2s$  threshold.

difference is evidently due to the interchannel coupling with a larger number of photoionization channels.

For the  $3d$  branching ratio, where the statistical value is 1.5, the branching ratio at 650 a.u. is a bit above 1.4, and it falls off much more slowly than that for the  $np$  cases, demonstrating that the relativistic effect on the wave functions is less important in the  $3d$  case. This occurs because the centrifugal barrier potential tends to keep the  $3d$  wave functions further away from the nucleus than the  $np$ , thereby causing the dipole matrix elements to be generated further from the nucleus than the  $np$  matrix elements. This, in turn, means that, in the  $3d$  case, the matrix elements are generated further away from the nucleus where the difference between  $3d_{5/2}$  and  $3d_{3/2}$  wave functions, in the region where the matrix element is generated, is not so considerably smaller than for the  $np$  cases.

Figure 8 depicts the Kr  $2p$ ,  $3p$ ,  $4p$ , and  $3d$  branching ratios in the neighborhood of the  $1s$  threshold and, like the case of Ar, interchannel coupling with the  $1s$  channels causes only very small changes, for reasons discussed in connection with Ar. The changes in the  $np$  and  $3d$  ratios are of about the same size, so there does not appear to be an angular momentum effect here. Figure 9 shows the same in the vicinity of the  $2s$  thresholds and the situation is rather different from the

$1s$  vicinity. Here the branching ratios are all increasing, as functions of energy and, even without coupling to the  $2s$  channels, the ratio is increasing. This seems to be at odds with the relativistic effect that causes the ratios to decrease with increasing energy and, since the ratio is increasing even without coupling with the  $2s$  channels, something else must be going on; a similar effect was seen earlier in Xe calculations [22]. It is known from earlier work that the interchannel coupling can affect cross sections and branching ratios over a broad range [22,23], so perhaps this phenomenology results from coupling with other channels; we shall come back to this point.

Figure 10 presents the branching ratios in the vicinity of the  $2p$  thresholds which are sufficiently split to accommodate significant interchannel coupling activity between the thresholds. This is seen in the  $3p$ ,  $4p$ , and  $3d$  branching ratios, and they are qualitatively the same for  $np$  and  $3d$  subshells, i.e., independent of angular momentum. Also shown in Fig. 10 are the branching ratios resulting from truncated calculations omitting (a) the coupling with all of the  $2p$  channels, (b) the coupling with  $2p_{3/2}$  channels, and (c) the coupling with the  $2p_{1/2}$  channels. Clearly the structure in the  $3p$  and  $4p$  branching ratios are caused by the coupling with the  $2p$  channels

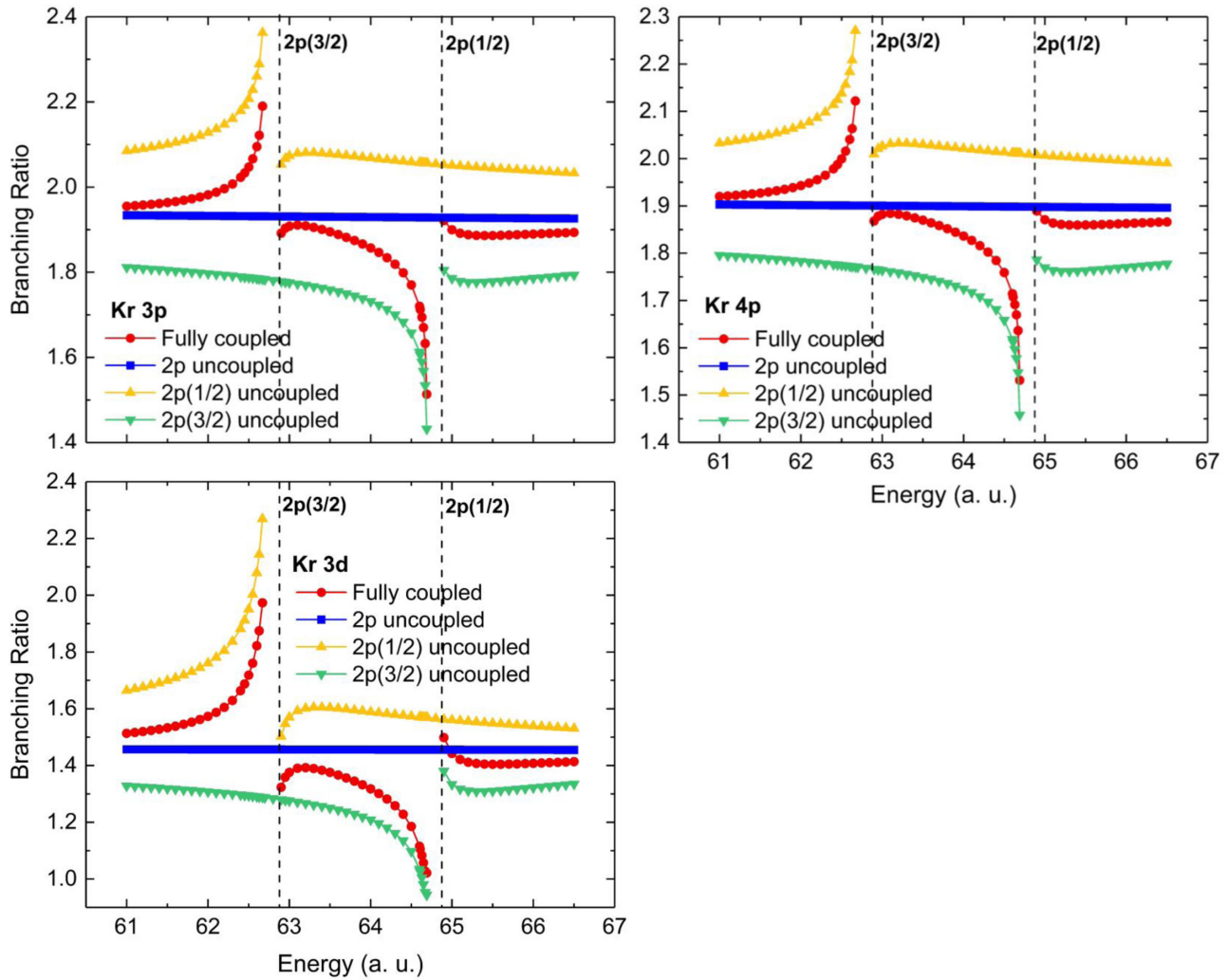


FIG. 10. Photoionization cross section branching ratios for Kr  $np_{3/2}/np_{1/2}$  and  $3d_{5/2}/3d_{3/2}$  in the vicinity of the Kr  $2p$  thresholds calculated using RRPA with full coupling (red dots) and truncated RRPA omitting the coupling with the  $2p$  photoionization channels (blue squares), omitting the coupling with  $2p_{1/2}$  channels (yellow triangles), and omitting the coupling with  $2p_{3/2}$  channels (green inverted triangles). The vertical dashed lines indicate the  $2p$  thresholds.

since the result without those couplings is quite featureless in this energy region.

Furthermore, it is evident from the truncated branching ratios that the coupling with  $2p_{3/2}$  channels is primarily responsible for the structure in the vicinity of the  $2p_{3/2}$  threshold, and similarly for  $2p_{1/2}$ . Above the  $2p_{1/2}$  thresholds, the fully coupled branching ratios drop, then start to rise, as a function of energy; the drop and the rise are clearly due to the interchannel coupling with the  $2p$  channels since the uncoupled branching ratios are monotone decreasing in this region. This rise in the branching ratios suggests what might be causing the branching ratios to rise in the vicinity of the  $2s$  thresholds, since they are not far away energetically. In Fig. 11, the  $3p$ ,  $4p$ , and  $3d$  branching ratios are shown over an extended region covering both the  $2p$  and  $2s$  thresholds, and the source of the peculiar behavior around the  $2s$  threshold is evident; coupling with the  $2p$  channels causes the branching ratios to rise in the vicinity of the  $2s$  threshold. Omitting that coupling with all  $2p$  and  $2s$  channels is seen to result in a smooth monotone decreasing branching ratio, in each

case, over the entire energy range shown. This demonstrates that, as previously seen in other contexts [22,23], interchannel coupling is operative over a broad range of energies and not merely in a small region around the subshell threshold. In this case, coupling with  $2p$  channels is crucial in the vicinity of the  $2s$  threshold, even though the  $2p$  thresholds are several hundred eV away.

The  $4p$  and  $3d$  branching ratios are depicted in the vicinity of the  $3p$  and  $3s$  thresholds in Fig. 12 along with the truncated results in which coupling with the  $3p$  and  $3s$  channels is omitted. As seen, the effects of the coupling are quite small indeed, on both the  $4p$  and  $3d$  results. Of interest, however, is that the  $3d$  branching ratio is monotone decreasing for both the fully coupled results (except for the resonance regions below each threshold) and the truncated results. The  $4p$  branching ratio is larger than the statistical value and increasing in this region. These are essentially threshold effects at such low energies where all sorts of correlations affect the branching ratios strongly, as seen in Fig. 7 for Kr.

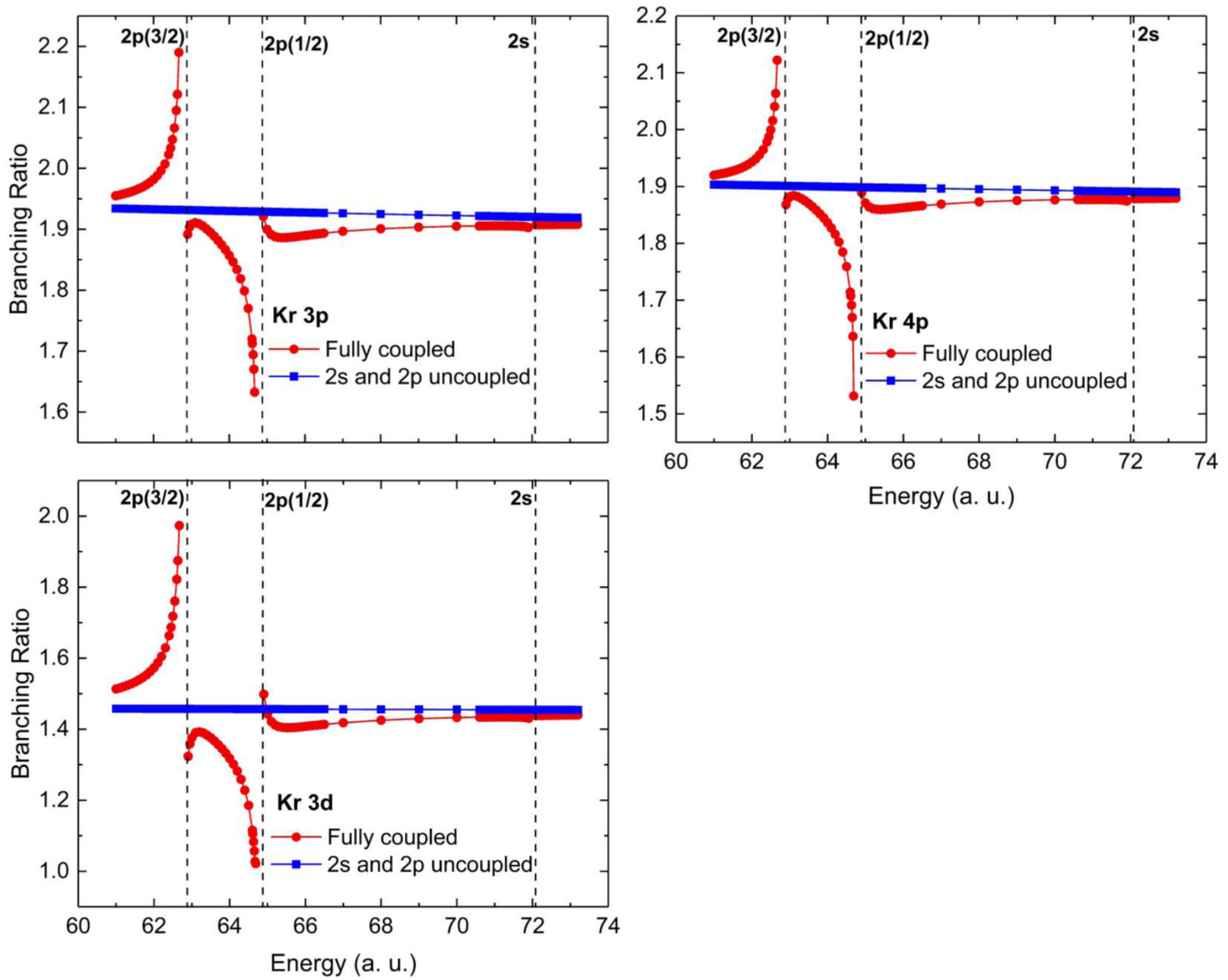


FIG. 11. Photoionization cross section branching ratios for Kr  $np_{3/2}/np_{1/2}$  and  $3d_{5/2}/3d_{3/2}$  in the vicinity of the Kr 2p and 2s thresholds calculated using RRPA with full coupling (red dots) and truncated RRPA omitting the coupling with the 2p and 2s photoionization channels (blue squares). The vertical dashed lines indicate the 2p and 2s thresholds.

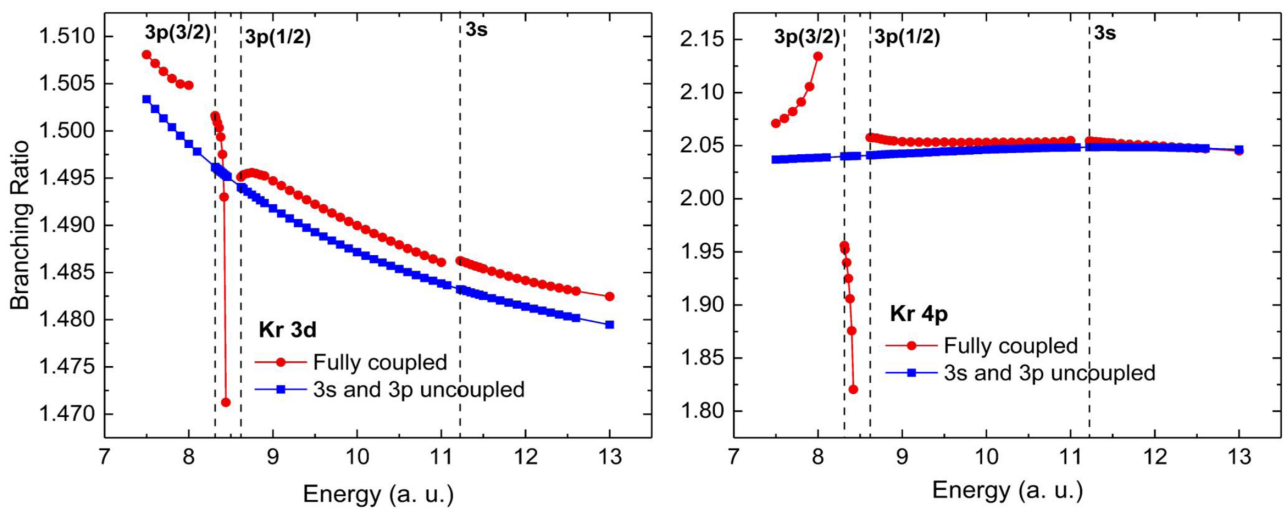


FIG. 12. Photoionization cross section branching ratios for Kr  $3d_{5/2}/3d_{3/2}$  in the vicinity of the Kr 3p and 3s thresholds calculated using RRPA with full coupling (red squares) and truncated RRPA omitting the coupling with the 3p and 3s photoionization channels (blue dots). The vertical dashed lines indicate the 3p and 3s thresholds.

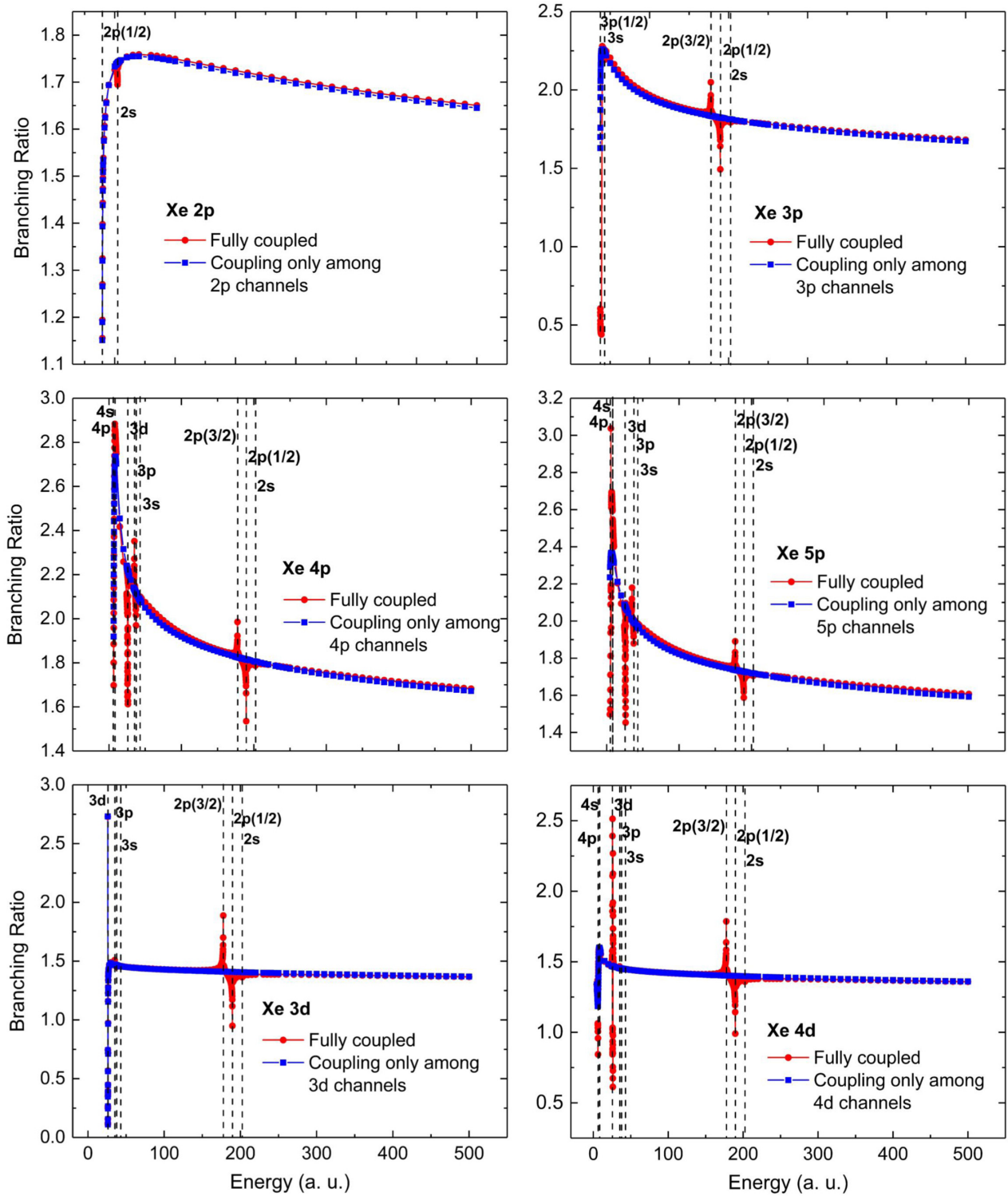


FIG. 13. Photoionization cross section branching ratios for Xe  $np_{3/2}/np_{1/2}$  and  $nd_{5/2}/nd_{3/2}$  calculated using RRPAs with full coupling (red dots) and with only intrashell coupling (blue squares). The vertical dashed lines indicate the thresholds.

#### D. Xenon

The Xe calculations include all of the photoionization channels from  $2s$ ,  $2p$ ,  $3s$ ,  $3p$ ,  $3d$ ,  $4s$ ,  $4p$ ,  $4d$ ,  $5s$ , and  $5p$  subshells, a total of 40 coupled relativistic channels; as mentioned previously, the  $1s$  threshold, being so deeply bound (over 1200 a.u.), is essentially irrelevant at the photon energies

we consider. An overall view of the branching ratios of the  $2p$ ,  $3p$ ,  $4p$ ,  $5p$ ,  $3d$ , and  $4d$  is given in Fig. 13. For the  $np$  states, at the highest energies of about 500 a.u., the branching ratios are about 1.7, continuing the trend seen for Ne, Ar, and Kr that the asymptotic branching ratios decrease with nuclear charge owing to the increased relativistic effects associated

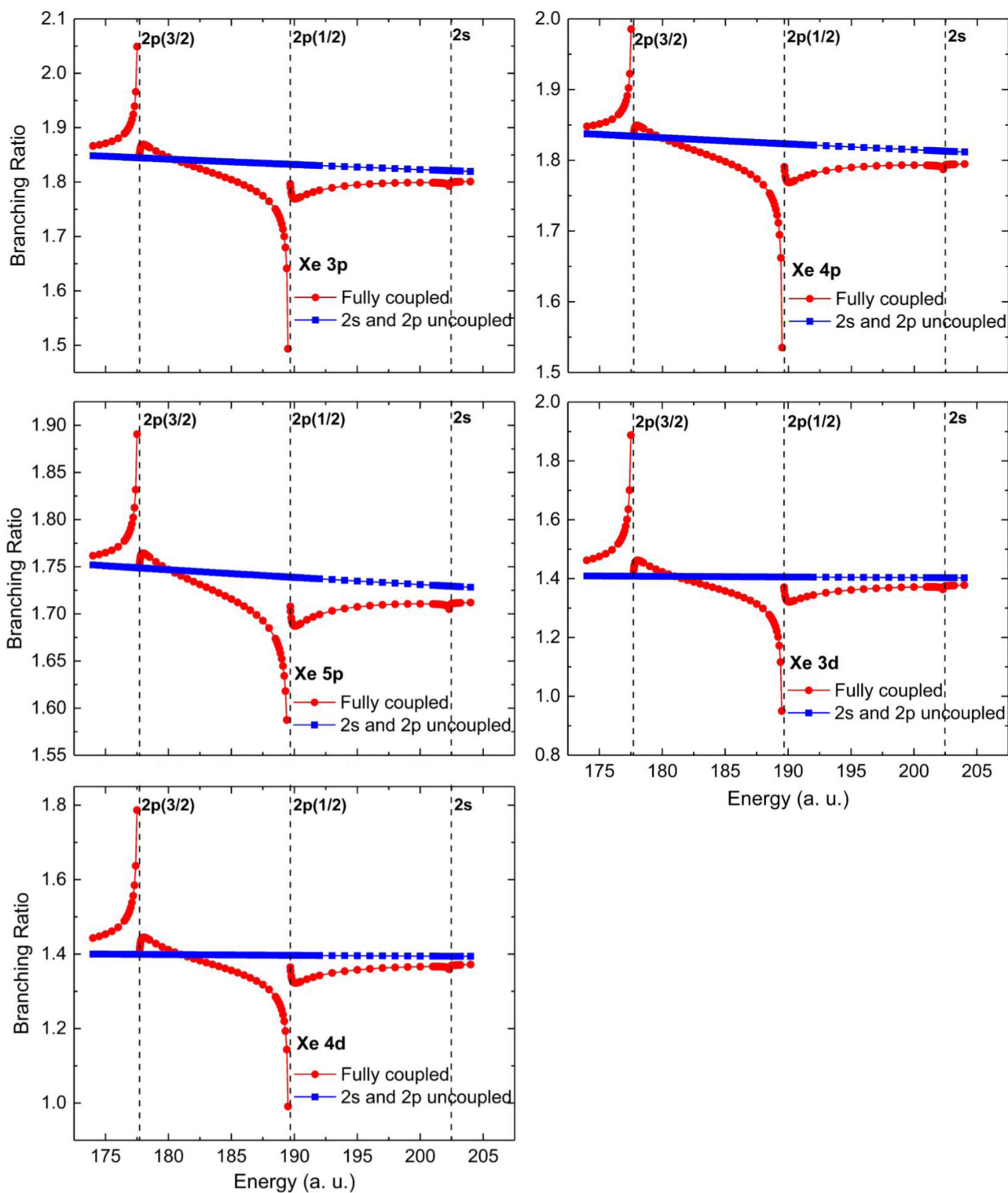


FIG. 14. Photoionization cross section branching ratios for Xe  $np_{3/2}/np_{1/2}$  and  $nd_{5/2}/nd_{3/2}$  in the vicinity of the Xe  $2p$  and  $2s$  thresholds calculated using RRPA with full coupling (red dots) and truncated RRPA omitting the coupling with the  $2p$  and  $2s$  photoionization channels (blue squares). The vertical dashed lines indicate the  $2p$  and  $2s$  thresholds.

with higher  $Z$ . Also, as seen and explained in the Ar case, the high-energy branching ratios are largely independent of principal quantum number  $n$  of the initial  $np$  or  $nd$  state. Reversing the trend seen for Ne, Ar, and Kr, the difference between the fully coupled branching ratios and the ones with

only coupling with the channels from the particular subshell (intrashell coupling) is slightly smaller than for Kr. This is due to the very complicated interchannel coupling interactions which can move the ratio in different directions, thereby partially canceling out. For the  $nd$  branching ratios, where the

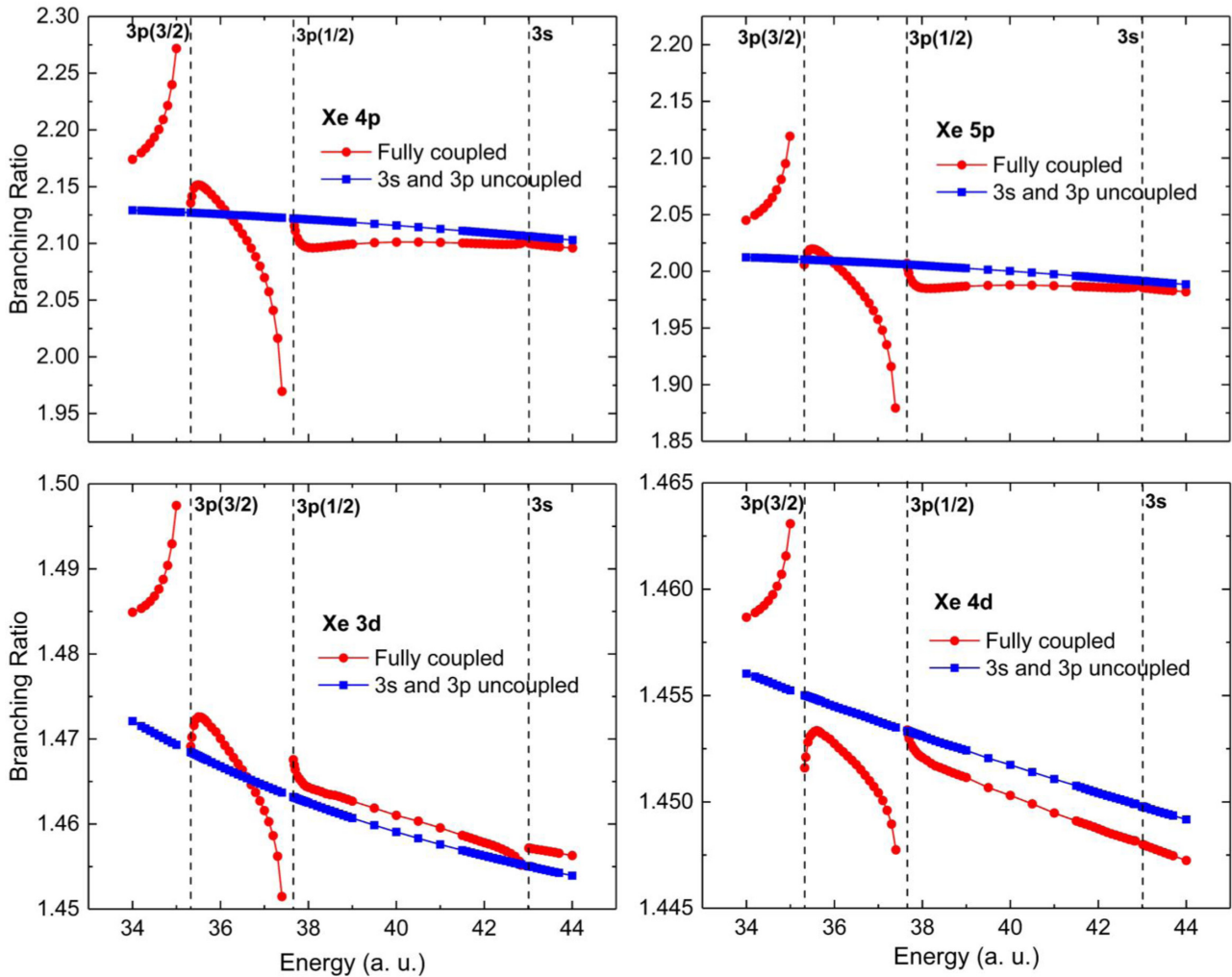


FIG. 15. Photoionization cross section branching ratios for Xe  $np_{3/2}/np_{1/2}$  and  $nd_{5/2}/nd_{3/2}$  in the vicinity of the Xe  $3p$  and  $3s$  thresholds calculated using RRPA with full coupling (red dots) and truncated RRPA omitting the coupling with the  $3p$  and  $3s$  photoionization channels (blue squares). The vertical dashed lines indicate the  $3p$  and  $3s$  thresholds.

statistical value is 1.5, the branching ratios at 500 a.u. are about 1.35, somewhat lower than the Kr case, as expected. And, as in the Kr case, the branching ratios fall off much more slowly than for the  $np$  cases; this demonstrates that the relativistic effect on the wave functions is less important for the  $nd$  cases, as explained for Kr. However, as in Kr, there are large excursions from smooth behavior in the vicinities of the inner-shell thresholds.

The Xe  $3p$ ,  $4p$ ,  $5p$ ,  $3d$ , and  $4d$  branching ratios are shown in the vicinity of the  $n = 2$  ( $2s$  and  $2p$ ) thresholds in Fig. 14 where the phenomenology is quite similar to the Kr branching ratios in the  $n = 2$  threshold region (Fig. 11) and for the same reasons. It is notable that the structure of the branching ratios in this region is not only the same for states of the same initial angular momentum independent of  $n$ , but also  $np$  and  $nd$  branching ratio structures are quite similar, and this was the case for Kr as well. This means that the interchannel coupling, which dominates the branching ratios in this region, affects  $np$  and  $nd$  states in a similar manner; we have no obvious explanation for this. It is also clear that, without the coupling to the  $n = 2$  photoionization channels, the branching ratios are monotone decreasing in this region, thereby showing that the

structure must be due to the coupling. A similar plot of the Xe  $4p$ ,  $5p$ ,  $3d$ , and  $4d$  branching ratios in the vicinity of the  $n = 3$  ( $3s$  and  $3p$ ) thresholds is given in Fig. 15. The phenomenology here is qualitatively like the branching ratios in the vicinity of the  $n = 2$  thresholds, however the excursions from the smooth background are seen to be smaller in magnitude. This reduced magnitude indicates that the interchannel coupling in the  $n = 3$  case is less relativistic than in the  $n = 2$  case; and this occurs because the  $3p$  and  $3s$  wave functions are less relativistic than their  $n = 2$  counterparts because the binding energy is much lower for the  $3p$  and  $3s$  states as compared to the  $2p$  and  $2s$ —about 40 a.u. as compared to about 200 a.u., respectively.

The branching ratios for Xe  $4p$ ,  $5p$ , and  $4d$  in the vicinity of the  $3d$  thresholds are particularly interesting, as noted earlier for  $4d$  [22], and are depicted in Fig. 16. In a small energy range in the vicinity of the  $3d$  thresholds the (fully coupled)  $np$  branching ratios vary significantly over a range of about 0.2 a.u. from 1.6 to 2.3 for  $4p$  and 1.4 to 2.1 for  $5p$ . Without the coupling to the  $3d$  photoionization channels, the branching ratios are seen to be smooth and monotone decreasing, thereby demonstrating that the sharp variations with

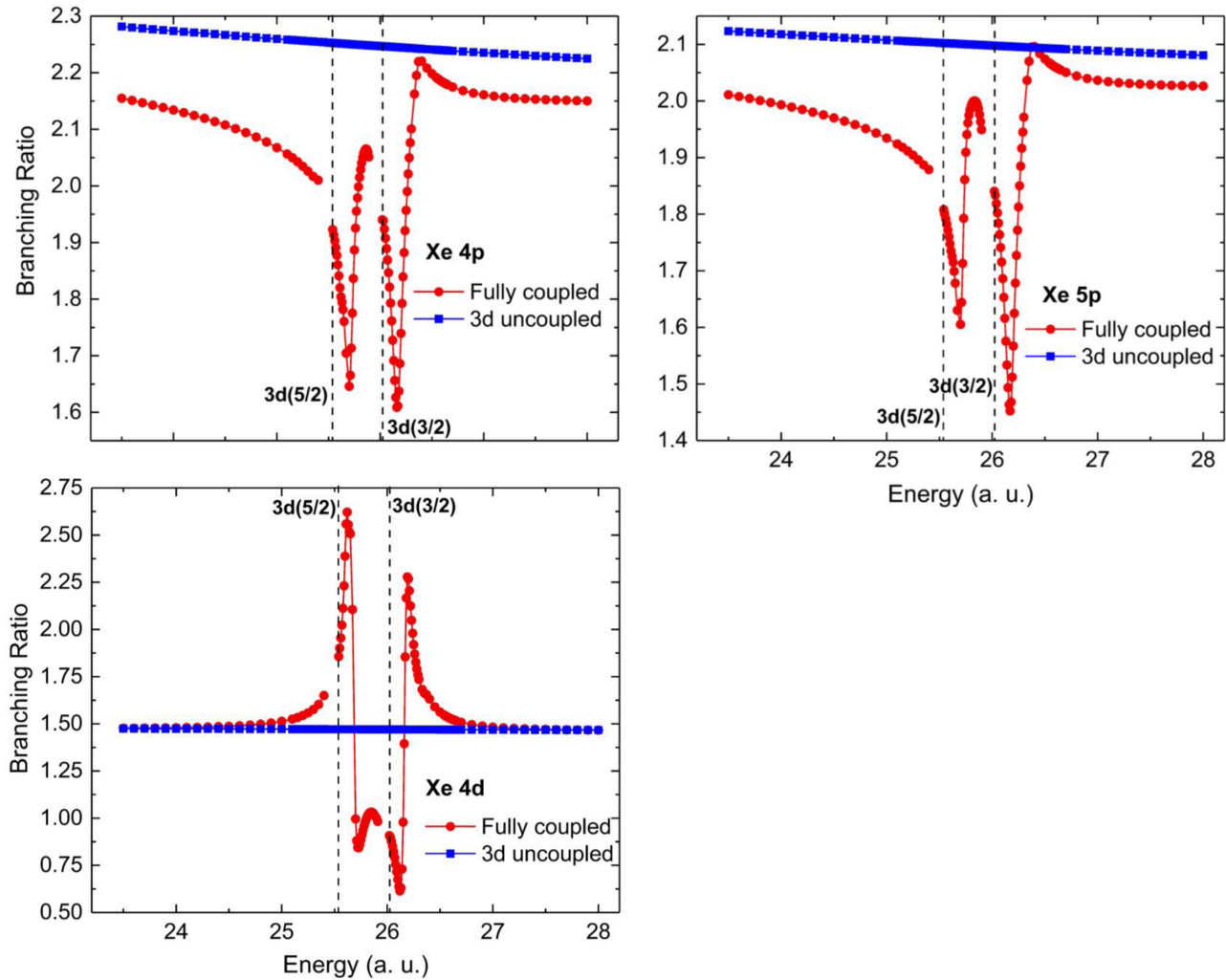


FIG. 16. Photoionization cross section branching ratios for Xe  $np_{3/2}/np_{1/2}$  and  $4d_{5/2}/4d_{3/2}$  in the vicinity of the Xe  $3d$  thresholds calculated using RRPA with full coupling (red dots) and truncated RRPA omitting the coupling with the  $3d$  photoionization channels (blue squares). The vertical dashed lines indicate the  $3d$  thresholds.

energy are entirely due to interchannel coupling. For the  $4d$  branching ratio the variations with energy are similar to the  $np$  case, but considerably larger over the same energy range; the  $4d$  branching is seen to vary over a range of about 2.0, from 0.6 to 2.6; again, the branching ratio with the  $3d$  coupling is smooth and monotone, indicating that in this case as well, it is the interchannel coupling that is responsible for the variation. That the variations in the branching ratio are so much larger for  $4d$  than for the  $np$  cases indicates that the interchannel coupling is considerably more important in the  $4d$  case. This occurs in this case because the angular part of the interchannel coupling matrix element is larger between channels of the same angular momenta vs channels with different angular momenta while, in the present case, the radial parts are about the same.

To understand these huge variations, which are similar in a general sense for Xe  $4p$ ,  $5p$ , and  $4d$ , we concentrate on the details for  $4d$  as an illustrative example. The calculated  $3d$  and  $4d$  cross sections are shown in Fig. 17 where it is seen that the maxima in the  $3d$  cross section are more than two orders of magnitude larger than the  $4d$  cross sections,

thus creating the conditions for significant changes to the  $4d$  cross sections via interchannel coupling. The  $3d$  cross sections show sharp maxima above the thresholds, shape resonances (or delay maxima) that were discovered many years ago [37,38]. In addition, the Xe  $3d_{5/2}$  cross section exhibits an extra small maximum at the energy of the  $3d_{3/2}$  shape resonance maximum. This was first discovered experimentally [39] and subsequently explained theoretically [40,41]; this phenomenon results from what is known as spin-orbit interaction activated interchannel coupling (SOIAC). Briefly, owing to the spin-orbit splitting of the  $3d$  thresholds, the  $3d_{3/2}$  delayed maximum occurs at an energy where the  $3d_{5/2}$  cross section is small, thereby transferring oscillator strength to the much smaller  $3d_{5/2}$  cross section via interchannel coupling and resulting in the feature seen in the  $3d_{5/2}$  cross section at about 26.2 a.u. The interchannel coupling of the  $3d$  cross sections with the  $4d$  channels then creates features in the  $4d$  cross sections at the same energies as the maxima in the  $3d$  cross sections as seen in Fig. 16. But it is also seen that the manifestation of the interchannel coupling in the two  $4d$  cross sections is rather different which shows that the

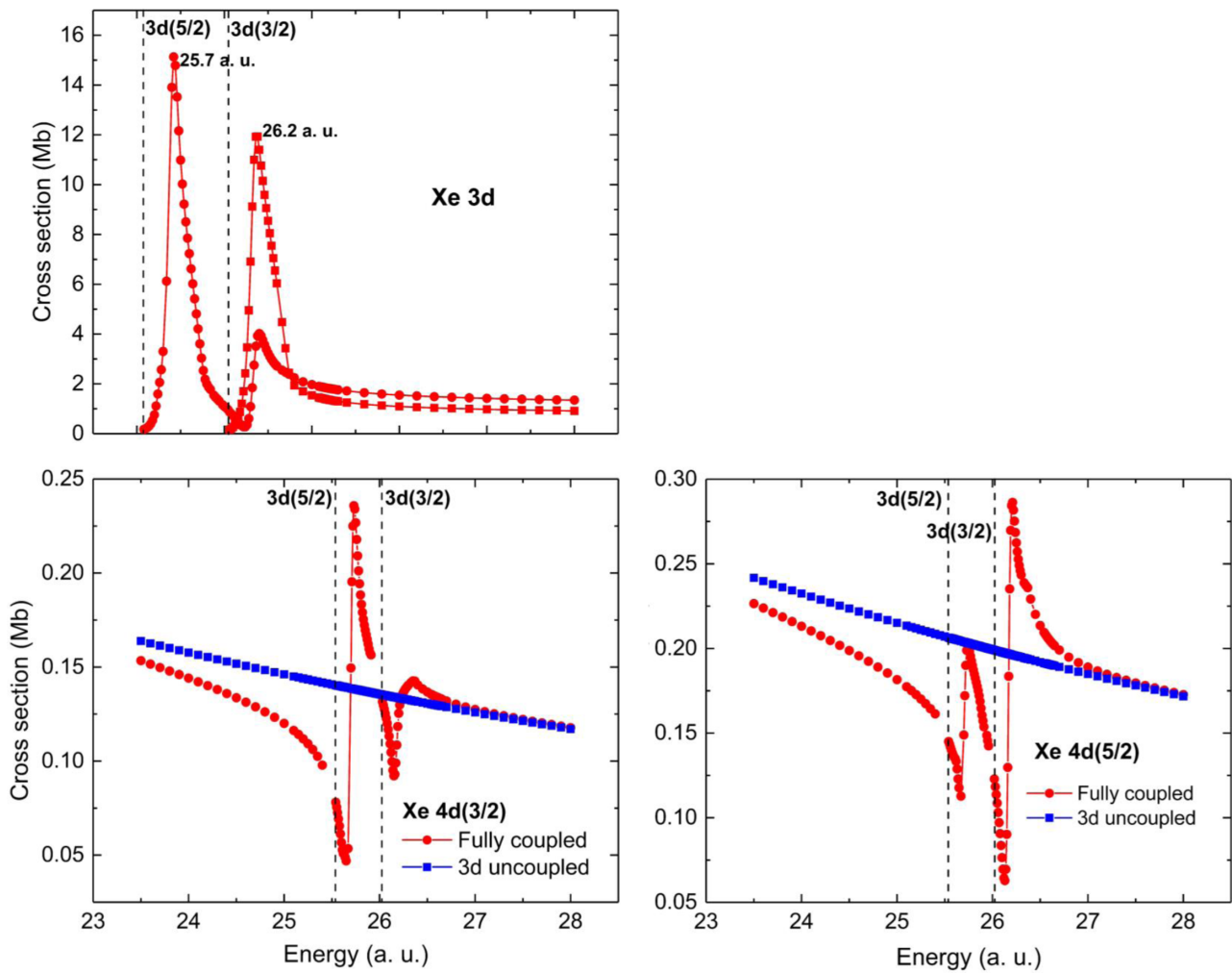


FIG. 17. Photoionization cross sections for Xe 3d (upper plot) and 4d (lower plots) in the vicinity of the Xe 3d thresholds calculated using RRPAs with full coupling (red dots) and truncated RRPAs omitting the coupling with the 3d photoionization channels (blue squares). The vertical dashed lines indicate the 3d thresholds.

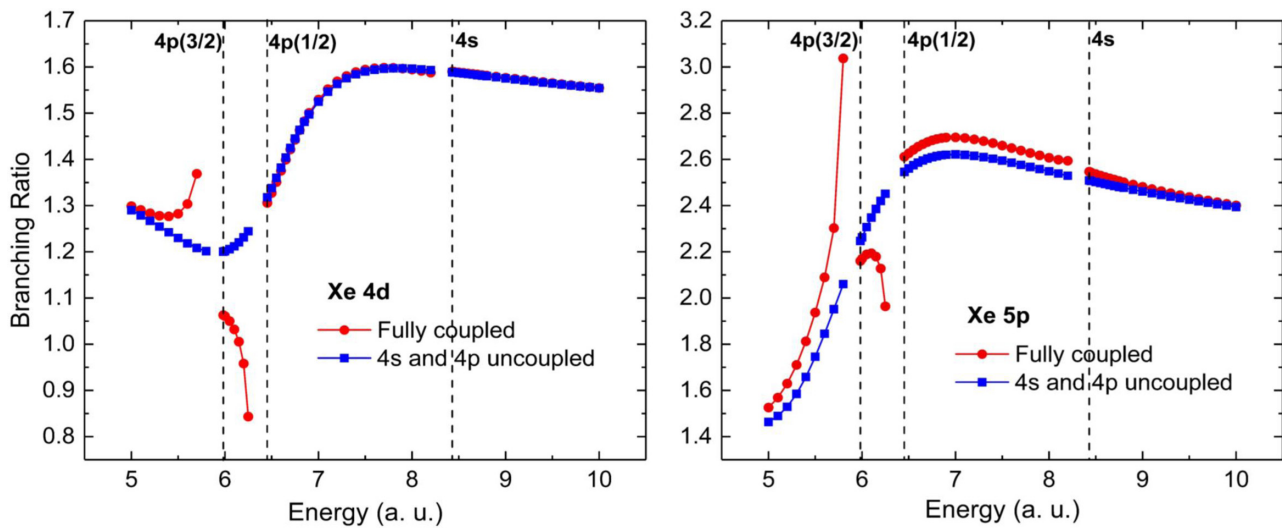


FIG. 18. Photoionization cross section branching ratios for Xe 4d and 5p in the vicinity of the Xe 3p and 4s thresholds calculated using RRPAs with full coupling (red dots) and truncated RRPAs omitting the coupling with the 4p and 4s photoionization channels (blue squares). The vertical dashed lines indicate the 4p and 4s thresholds.

interchannel coupling matrix elements are strongly  $j$  dependent, i.e., strongly affected by relativistic interactions. And this strong difference in cross sections explains the Xe  $4d$  branching ratio is seen to exhibit huge variations over this energy region of the  $3d$  thresholds (Fig. 16). The explanation of the variations in the Xe  $4p$  and  $5p$  branching ratios is essentially the same as for the  $4d$  case, although the details differ somewhat. However, the features of  $4p$  and  $5p$  branching ratios occur at essentially the same photon energies as for the  $4d$ , as seen in Fig. 16.

The  $4d$  and  $5p$  branching ratios in the vicinity of the  $4p$  and  $4s$  thresholds are shown in Fig. 18 where it is seen that, except for the resonance region just below the  $4p$  thresholds, the effect of interchannel coupling is relatively small. Above the  $4p_{1/2}$  threshold the  $4d$  branching ratio shows no effect at all of the interchannel coupling, while the  $5p$  branching ratio shows a small effect. This is a further indication that the interchannel coupling interaction between outer and inner photoionization channels of the same angular momentum,  $5p$  and  $4p$ , in this case, is typically stronger than the between channels of different angular momentum,  $4d$  and  $3p$  in the present case.

#### IV. SUMMARY AND CONCLUSIONS

A survey of the branching ratios of spin-orbit doublets of the noble gases, Ne, Ar, Kr, and Xe, has been conducted over a broad range of photon energies well above their thresholds. It was found that, well above the thresholds, the overall branching ratios do not approach the nonrelativistic limit, but all decrease with energy, as predicted theoretically many years ago [20,21] and confirmed experimentally in a few cases recently [22]. It has also been demonstrated that the falloff of the branching ratio with energy increases with  $Z$  resulting from the relativistic effects that cause the ratio of probability densities of the  $(j = l - 1)/(j = l + 1)$  wave functions for a spin-orbit doublet to behave as  $Z^2/r$  for small  $r$  [29]. It was found that, well above threshold, all  $np$  branching ratios fell off faster than  $nd$  owing to the stronger centrifugal repulsion for  $nd$  states that keeps the  $nd$  states further from the small  $r$  region where the wave functions are more relativistic. However, at high energy, the falloff of branching ratios of all  $np$  states was the same for a given atom, independent of  $n$ , and

the same was true for the  $nd$  states; this occurs because the wave functions of initial states of the same  $l$  but different  $n$  are essentially exactly the same at small  $r$  except for an overall normalization constant that cancels out in the branching ratios.

As suggested earlier [22,23] it was demonstrated that the branching ratios could be strongly affected in the vicinity of inner-shell thresholds through correlation in the final-state wave functions known as interchannel coupling; this showed that the interchannel coupling was different for the two members of a spin-orbit doublet, i.e., that the interchannel coupling was affected by relativistic interactions. It was further shown that the interchannel coupling matrix elements were largest between photoionization channels of the same initial state angular momentum. This was demonstrated most clearly in the  $4d$  branching ratio in the neighborhood of the  $3d$  thresholds. In addition, it should be reiterated that the results show that interchannel coupling is the major aspect of correlation that causes the branching ratios to deviate from single-particle behavior.

It is of interest reiterate that the physics not included in the present calculations, principally interchannel coupling with photoionization-plus-excitation channels, will affect the results at just the few percent level, owing to the smallness of the cross sections of the omitted multiple-excitation channels. This is further borne out by the agreement of the RRPA calculations with experiment as detailed in Ref. [22].

Finally, this work will be extended to higher  $Z$  atoms in the future to test the various conclusions that the present work has suggested. It will also be of interest to look at  $nf$  states to see if the same phenomenology is revealed. Other than the work of Ref. [22], there is no experimental work on the noble gas branching ratios at the higher energies. We hope the present paper will prompt new laboratory studies.

#### ACKNOWLEDGMENTS

This work was supported by the U.S. Department of Energy, Office of Basic Sciences, Division of Chemical Science, Geosciences and Biosciences under Grant No. DE-FG02-03ER15428. C.R.M. acknowledges the assistance of R. Hosseini and A. Razavee in modifying and running the various codes.

- 
- [1] A. F. Starace, in *Theory of Atomic Photoionization*, Handbuch der Physik Vol. 31 (Springer-Verlag, Berlin, 1982), pp. 1–121.
  - [2] R. H. Pratt, A. Ron, and H. K. Tseng, Atomic photoeffect above 10 keV, *Rev. Mod. Phys.* **45**, 273 (1973).
  - [3] I. P. Grant, *Relativistic Quantum Theory of Atoms and Molecules: Theory and Computation* (Springer, Berlin, 2007).
  - [4] W. R. Johnson and K. T. Cheng, Photoionization of the outer shells of neon, argon, krypton, and xenon using the relativistic random-phase approximation, *Phys. Rev. A* **20**, 978 (1979).
  - [5] Y. S. Kim, A. Ron, R. H. Pratt, B. R. Tambe, and S. T. Manson, Relativistic Effects in the Photoionization of High-Z Elements: Splitting and Shifts in Minima, *Phys. Rev. Lett.* **46**, 1326 (1981).
  - [6] P. C. Deshmukh, B. R. Tambe, and S. T. Manson, Relativistic effects in the photoionization of heavy atoms: Cooper minima, *Aust. J. Phys.* **39**, 679 (1986).
  - [7] A. Ron, I. B. Goldberg, J. Stein, S. T. Manson, R. H. Pratt, and R. Y. Yin, Relativistic, retardation and multipole effects in photoionization cross sections:  $Z, n, l$  dependence, *Phys. Rev. A* **50**, 1312 (1994).
  - [8] H. Wang, G. Snell, O. Hemmers, M. M. Sant'Anna, I. Sellin, N. Berrah, D. W. Lindle, P. C. Deshmukh, N. Haque, and S. T. Manson, Dynamical Relativistic Effects in Photoionization: Spinorbital-resolved Angular Distributions of Xenon 4d Photoelectrons Near the Cooper Minimum, *Phys. Rev. Lett.* **87**, 123004 (2001).

- [9] D. Toffoli, M. Stener, and P. Decleva, Application of the relativistic time-dependent density functional theory to the photoionization of xenon, *J. Phys. B: Atomic, Molecular, and Optical Phys.* **35**, 1275 (2002).
- [10] D. Cubaynes, H.-L. Zhou, N. Berrah, J.-M. Bizau, J. D. Bozek, S. Canton, S. Diehl, X.-Y. Han, A. Hibbert, E. T. Kennedy, S. T. Manson, L. Voky, and F. J. Wuilleumier, Dynamical and relativistic effects in experimental and theoretical studies of inner-shell photoionization of sodium, *J. Phys. B* **40**, F121 (2007).
- [11] S. Saha, J. Jose, S. Saha, H. R. Varma, P. C. Deshmukh, A. S. Kheifets, V. K. Dolmatov, and S. T. Manson, Relativistic effects in photoionization time delay near the cooper minimum of noble gas atoms, *Phys. Rev. A* **90**, 053406 (2014).
- [12] A. Kheifets, A. Mandal, P. C. Deshmukh, V. K. Dolmatov, D. A. Keating, and S. T. Manson, Relativistic calculations of angular dependent photoemission time delay, *Phys. Rev. A* **94**, 013423 (2016).
- [13] T. Kjellsson Lindblom, M. Førre, E. Lindroth, and S. Selstø, Relativistic effects in photoionizing a circular rydberg state in the optical regime, *Phys. Rev. A* **102**, 063108 (2020).
- [14] A. K. Razavi, R. K. Hosseini, D. A. Keating, P. C. Deshmukh, and S. T. Manson, Photoionization of superheavy Atoms: Correlation and relativistic effects, *J. Phys. B* **53**, 205203 (2020).
- [15] J. Berkowitz, *Photoabsorption, Photoionization, and Photoelectron Spectroscopy* (Academic, New York, 1979).
- [16] T. E. H. Walker, J. Berkowitz, J. L. Dehmer, and J. T. Waber, Nonstatistical Ratios of Photoionization Cross Sections for States Split by Spin-Orbit Coupling, *Phys. Rev. Lett.* **31**, 678 (1973).
- [17] F. Wuilleumier, M. Y. Adam, P. Dhez, N. Sandner, V. Schmidt, and W. Mehlhorn, Energy dependence of the photoelectron branching ratio in the 5p shell of xenon, *Phys. Rev. A* **16**, 646 (1977).
- [18] G. L. Goodman and J. Berkowitz, Partial cross sections in the photoionization of open-shell atoms: Photoelectron spectroscopy of Te, *J. Chem. Phys.* **94**, 321 (1991).
- [19] D. Di Tommaso and P. Decleva, Branching ratio deviations from statistical behavior in core photoionization, *J. Chem. Phys.* **123**, 064311 (2005).
- [20] A. Ron, Y. S. Kim, and R. H. Pratt, Subshell branching ratios of partial photoionization cross sections, *Phys. Rev. A* **24**, 1260 (1981).
- [21] Y. S. Kim, R. H. Pratt, and A. Ron, Nonstatistical behavior of photoeffect subshell branching ratios at high energies, *Phys. Rev. A* **24**, 1889 (1981).
- [22] R. Püttner, J. B. Martins, T. Marchenko, O. Travnikova, R. Guillemin, L. Journel, I. Ismail, G. Goldsztejn, D. Koulentianos, D. Céolin, M. L. Rocco, M. N. Piancastelli, M. Simon, D. A. Keating, C. R. Munasinghe, P. C. Deshmukh, and S. T. Manson, Nonstatistical behavior of the photoionization of spin-orbit doublets, *J. Phys. B* **54**, 085001 (2021).
- [23] W. Drube, T. M. Grehk, S. Thiess, G. B. Pradhan, H. R. Varma, P. C. Deshmukh, and S. T. Manson, Pronounced effects of interchannel coupling in high-energy photoionization, *J. Phys. B* **46**, 245006 (2013).
- [24] W. R. Johnson and C. D. Lin, Multichannel relativistic random-phase approximation for the photoionization of atoms, *Phys. Rev. A* **20**, 964 (1979).
- [25] W. R. Johnson, C. D. Lin, K. T. Cheng, and C. M. Lee, Relativistic random-phase approximation, *Phys. Scr.* **21**, 409 (1980).
- [26] E. W. B. Dias, H. S. Chakraborty, P. C. Deshmukh, S. T. Manson, O. Hemmers, P. Glans, D. L. Hansen, H. Wang, S. B. Whitfield, D. W. Lindle, R. Wehlitz, J. C. Levin, I. A. Sellin, and R. C. C. Perera Breakdown of the Independent Particle Approximation in High-Energy Photoionization, *Phys. Rev. Lett.* **78**, 4553 (1997).
- [27] D. L. Hansen, O. Hemmers, H. Wang, D. W. Lindle, I. A. Sellin, H. S. Chakraborty, P. C. Deshmukh, and S. T. Manson, Validity of the independent-particle approximation in x-ray Photoemission: The Exception, not the rule, *Phys. Rev. A* **60**, R2641 (1999).
- [28] G. B. Armen and F. P. Larkins, Valence Auger and X-ray participator and spectator processes for neon and argon atoms, *J. Phys. B* **24**, 741 (1991), and references therein.
- [29] H. A. Bethe and E. E. Salpeter, in *Quantum Mechanics of One- and Two-Electron Atoms* (Springer, Berlin, 1957), pp. 63–71.
- [30] E. W. B. Dias, H. S. Chakraborty, P. C. Deshmukh, and S. T. Manson, Relativistic effects in the photoionization of atomic beryllium, *J. Phys. B* **32**, 3383 (1999).
- [31] H.-C. Chi and K.-N. Huang, Photoionization of beryllium in the multiconfiguration relativistic random-phase approximation, *Phys. Rev. A* **43**, 2542 (1991).
- [32] W.-C. Chu, H.-L. Zhou, A. Hibbert, and S. T. Manson, Photoionization of the Be isoelectronic sequence, *J. Phys. B* **42**, 205003 (2009).
- [33] R. H. Pratt and H. K. Tseng, Behavior of electron wave functions near the atomic nucleus and normalization screening theory in the atomic photoeffect, *Phys. Rev. A* **5**, 1063 (1972).
- [34] Y. S. Kim, Normalization screening theory manifested in photoeffect, *Radiat. Phys. Chem.* **59**, 145 (2000).
- [35] F. A. Parpia, W. R. Johnson, and V. Radojević, Application of the relativistic local-density approximation to photoionization of the outer shells of neon, argon, krypton, and xenon, *Phys. Rev. A* **29**, 3173 (1984).
- [36] [https://physics.nist.gov/PhysRefData/ASD/levels\\_form.html](https://physics.nist.gov/PhysRefData/ASD/levels_form.html).
- [37] S. T. Manson and J. W. Cooper, Photo-ionization in the soft x-ray range: 1Z dependence in a central-potential model, *Phys. Rev.* **165**, 126 (1968).
- [38] R. D. Deslattes, Photoionization of the M Shell of Xenon, *Phys. Rev. Lett.* **20**, 483 (1968).
- [39] A. Kivimäki, U. Hergenthal, B. Kempgens, R. Hentges, M. N. Piancastelli, K. Maier, A. Rüdell, J. J. Tulkki, and B. M. Bradshaw, Near-threshold study of Xe 3d photoionization, *Phys. Rev. A* **63**, 012716 (2000).
- [40] M. Ya. Amusia, L. V. Chernysheva, S. T. Manson, A. Z. Msezane, and V. Radojević, Strong Electron Correlation in Photoionization of Spin Orbit Doublets, *Phys. Rev. Lett.* **88**, 093002 (2002).
- [41] V. Radojević, D. M. Davidovic, and M. Ya, Amusia, Near-threshold photoionization of the Xe 3d spin-orbit doublet: Relativistic, relaxation, and intershell interaction effects, *Phys. Rev. A* **67**, 022719 (2003).